Mineralogical Magazine, November 2014, Vol. 78(6), pp. 1405–1416

OPEN ACCESS

The experimental determination of hydromagnesite precipitation rates at 22.5–75ºC

U.-N. Berninger[1,2,*], G. Jordan[2], J. Schott[1] and E. H. Oelkers[1,3]

[1] Géoscience Environnement Toulouse, CNRS-UPS-OMP, 14 av. Édouard Belin, 31400 Toulouse, France
[2] Department für Geo- und Umweltwissenschaften, LMU, Theresienstr. 41, 80333 München, Germany
[3] Department of Earth Sciences, UCL, Gower Street, London WC1E 6BT, UK

[*Received 18 July 2014; Accepted 17 October 2014; Associate Editor: T. Stawski*]

ABSTRACT

Natural hydromagnesite ($Mg_5(CO_3)_4(OH)_2{\cdot}4H_2O$) dissolution and precipitation experiments were performed in closed-system reactors as a function of temperature from 22.5 to 75ºC and at 8.6 < pH < 10.7. The equilibrium constants for the reaction $Mg_5(CO_3)_4(OH)_2{\cdot}4H_2O + 6H^+ = 5Mg^{2+} + 4HCO_3^- + 6H_2O$ were determined by bracketing the final fluid compositions obtained from the dissolution and precipitation experiments. The resulting constants were found to be $10^{33.7\pm0.9}$, $10^{30.5\pm0.5}$ and $10^{26.5\pm0.5}$ at 22.5, 50 and 75ºC, respectively. Whereas dissolution rates were too fast to be determined from the experiments, precipitation rates were slower and quantified. The resulting BET surface area-normalized hydromagnesite precipitation rates increase by a factor of ~2 with pH decreasing from 10.7 to 8.6. Measured rates are approximately two orders of magnitude faster than corresponding forsterite dissolution rates, suggesting that the overall rates of the low-temperature carbonation of olivine are controlled by the relatively sluggish dissolution of the magnesium silicate mineral.

Keywords: hydromagnesite, carbon storage, carbonate minerals, precipitation.

Introduction

The precipitation rates of carbonate minerals are of current interest due to their potential role in carbon storage (e.g. Seifritz, 1990; Lackner *et al*., 1995; Xu *et al*., 2005; Marini, 2007; Flaathen *et al*., 2011). Carbon storage *via* carbonate mineral precipitation appears to be particularly favoured in basaltic and ultramafic rocks due to their high reactivity and the prevalence of divalent cations such as Ca^{2+} and Mg^{2+} (McGrail *et al*., 2006; Alfredsson *et al*., 2008; Oelkers *et al*., 2008; Matter *et al*., 2009, 2011; Schaef *et al*., 2010, 2011; Gislason *et al*., 2010; Gysi and Stefansson, 2012; Aradóttir *et al*., 2012; Oskierski *et al*., 2013; Gislason and Oelkers, 2014). Whereas anhydrous calcium carbonates such as calcite and aragonite precipitate readily at ambient temperatures (e.g. Burton and Walter, 1987; Zuddas and Mucci, 1998; Teng *et al*., 2000; Lakshtanov and Stipp, 2010; Rodriguez-Blanco *et al*., 2011; Ruiz-Agudo *et al*., 2013), the precipitation of the anhydrous Mg-carbonate mineral magnesite is apparently inhibited at temperatures of <~80ºC (e.g. Saldi *et al*., 2009, 2012). At these lower temperatures, the precipitation of hydrous Mg carbonates, such as hydromagnesite and dypingite are favoured (Mavromatis *et al*., 2012; Shirokova *et al*., 2013). The goal of the present study was an improved understanding of the precipitation kinetics of hydrous magnesium carbonate minerals at temperatures below 80ºC, in part to assess their potential to store carbon at

* E-mail: berninger@get.obs-mip.fr
DOI: 10.1180/minmag.2014.078.6.07

This paper is published as part of a special issue in *Mineralogical Magazine*, Vol. **78(6)**, 2014 entitled 'Mineral–fluid interactions: scaling, surface reactivity and natural systems'.

ambient temperatures. Hydromagnesite growth rates were measured in closed-system reactors at 22.5–75ºC. The results of these experiments are used here to evaluate the potential of hydrous magnesium carbonate minerals as a carbon-storage host.

Theoretical background

The standard state adopted in this study for thermodynamic calculations is that of unit activity for pure minerals and H_2O at any temperature and pressure. For aqueous species other than H_2O, the standard state is unit activity of the species in a hypothetical 1 molal solution referenced to infinite dilution at any temperature and pressure. Hydromagnesite dissolution can be described using:

$$Mg_5(CO_3)_4(OH)_2{\cdot}4H_2O + 6H^+ = 5Mg^{2+} + 4HCO_3^- + 6H_2O \quad (1)$$

Taking account of this standard state, the law of mass action for reaction 1 is given by:

$$K_{Hmg} = \frac{a^5_{Mg^{2+}} \cdot a^4_{HCO_3^-}}{a^6_{H^+}} \quad (2)$$

where K_{Hmg} stands for the equilibrium constant of reaction 1 and a_i represents the activity of the subscripted aqueous species. The chemical affinity (A) of reaction 1 can be expressed as:

$$A = -RT \ln \left(\frac{IAP_{Hmg}}{K_{Hmg}} \right) = -RT \ln \Omega_{Hmg} \quad (3)$$

where R is the gas constant (= 8.3144 J/Kmol), T is absolute temperature, IAP_{Hmg} represents the aqueous ion activity product, and Ω_{Hmg} represents the saturation state of the aqueous phase with respect to hydromagnesite. All thermodynamic calculations in this study were performed using the *PHREEQC for Windows* (Version 2.18) computer code (Parkhurst and Appelo, 1999) together with its llnl database after adding the equilibrium constants for Mg^{2+} hydrolysis and the carbonic acid dissociation reported by Brown *et al*. (1996) and Millero *et al*. (2007), respectively.

Materials and methods

Natural hydromagnesite ($Mg_5(CO_3)_4(OH)_2{\cdot}4H_2O$) was collected as stromatolite precipitates from Lake Salda in southwest Turkey (cf. Shirokova *et al*., 2011) then hand-milled with an agate mortar and pestle. The resulting powder was cleaned with H_2O_2 to remove organics and oven dried at 50ºC for 24 h. The particles were not cleaned ultrasonically due to the fine nature of these natural grains. Scanning Electron Microscope (SEM) images, obtained using a JEOL JSM-6360 LV microscope, of the resulting hydromagnesite are shown in Fig. 1. The hydromagnesite powder prepared consists of agglomerated crystals. The size of the individual hydromagnesite crystals ranges up to ~5 μm, the agglomerates range up to 50 μm. No other mineral phases were evident from SEM images nor were any detected using backscattered electron microscopy. The purity of this

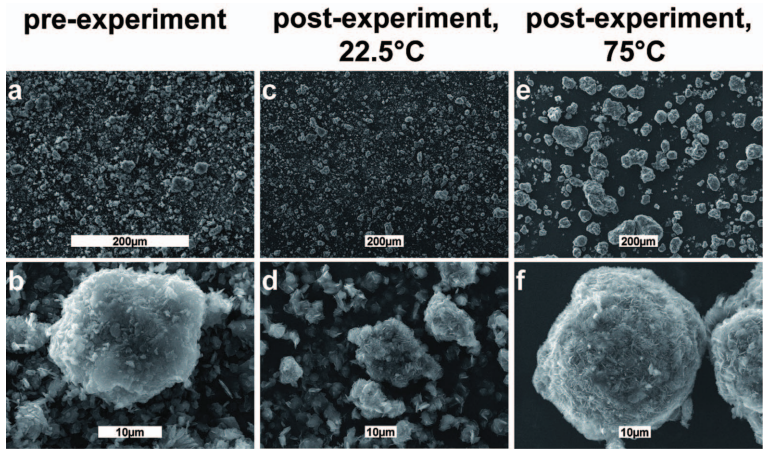

FIG. 1. SEM images of the initial hydromagnesite seed material (*a*,*b*), after the precipitation experiment at 22.5ºC at pH 10.72 (*c*,*d*), and after the experiment performed at 75ºC at pH 9.75 (*e*,*f*).

https://doi.org/10.1180/minmag.2014.078.6.07 Published online by Cambridge University Press

hydromagnesite was further verified by X-ray diffraction using an INEL CPS-120 diffractometer with Co$K\alpha$ radiation, λ = 1.78897 Å, and a graphite monochromator. X-ray diffraction was performed from 1 to 110º2θ at 0.09º2θ/min and at a step size of 0.029º2θ. This analysis revealed no phase other than hydromagnesite. The surface area of the hydromagnesite prepared was determined to be 8.5 $m^2/g \pm 10\%$ by multipoint krypton adsorption according to the BET method (Brunauer *et al*., 1938) using a Quantachrome Gas Sorption system.

Hydromagnesite dissolution and precipitation experiments were performed in closed-system 0.5 l high-density polypropylene reactors. Approximately 1 g of hydromagnesite powder and 500 g of an aqueous sodium carbonate buffer solution with ionic strength of 0.1 mol/kg were placed into each reactor. The reactors were subsequently sealed and placed in temperature-controlled shaking water baths. The initial solutions were composed of deionized H_2O and Merck reagent-grade Na_2CO_3 and $NaHCO_3$ at varying ratios (Table 1); the resulting aqueous solutions had a pH ranging from 7.7 to 11.2. The original hydromagnesite was allowed to dissolve in this fluid for about 5 days until a steady-state aqueous Mg concentration was attained and validated. After this time, ~3 g of a 1.81 mol/kg aqueous $MgCl_2$ solution was added to each reactor to supersaturate the fluid with respect to hydromagnesite.

The fluid in each reactor was sampled regularly to monitor reaction progress. The reactive fluid Mg concentration was measured by flame atomic absorption spectroscopy using a Perkin Elmer Zeeman 5000 Atomic Absorption Spectrometer with an uncertainty of ±2% and a detection limit of 6×10^{-7} mol/kg. Alkalinity was determined by standard HCl titration using Schott TA 10plus with an uncertainty of ±2% and a detection limit of 5×10^{-5} eq/l. Fluid pH measurements were performed at 22.5ºC immediately after sampling using a standard glass electrode, previously calibrated with 4.01, 6.86 and 9.18 NIST pH buffers.

Results

Aqueous Mg concentrations as a function of time during a representative experiment are illustrated in Fig. 2. An approximately constant Mg concentration was obtained by dissolution within ~30 min. Following the addition of $MgCl_2$ to the fluid phase, the aqueous Mg concentration decreased systematically with time. Note the near-constant aqueous Mg concentration attained at the end of the dissolution leg is distinct from that attained at the end of the precipitation leg of the experiment, reflecting the different fluid pH present during these legs.

The rate at which steady-state was attained during hydromagnesite dissolution was too rapid

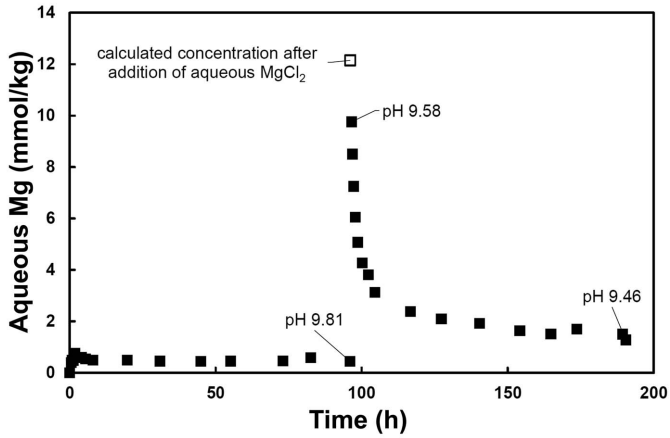

FIG. 2. Temporal evolution of aqueous Mg concentration for a representative experiment performed at 50ºC. This experiment began by the dissolution of hydromagnesite until a near-stationary state was attained. After 100 h, additional Mg was added to the aqueous fluid and precipitation began. Uncertainties in the concentration measurements are within the size of the symbols. Note that steady-state concentration of aqueous Mg during the dissolution leg is reached in <30 min. The initial and final pH values of the fluid during the dissolution and precipitation leg of the experiment are shown.

https://doi.org/10.1180/minmag.2014.078.6.07 Published online by Cambridge University Press

TABLE 1. Summary of experimental data.

T	Hydromagnesite seeds	Composition of buffer solution		– Experimental parameters at the – final state of the dissolution leg				Addition of $MgCl_2$	—— Experimental parameters at the final state —— of precipitation leg				
(ºC)	(g)	$NaHCO_3$ (g/l)	Na_2CO_3 (g/l)	pH	Mg (mmol/kg)	alk (mol/l)	log *IAP*	(1.81 mol/kg) (g)	pH	Mg (mmol/kg)	alk (mol/l)	log *IAP*	k (10^9·mol/m^2/s)
22.5	0.9506	8.8990[a]	0	8.75	5.19	0.114	32.94	2.89	8.59	14.6	0.105	34.47	1.0
22.5	0.9515	8.8992	0	8.85	4.15	0.128	32.89	2.89	8.65	13.5	0.107	34.56	1.0
22.5	0.9515	8.3166	0.2757	8.92	3.29	0.113	32.64	2.91	8.72	12.7	0.104	34.67	1.0
22.5	0.9498	6.9732	0.8479	9.14	2.30	0.104	32.61	2.79	8.86	9.85	0.0944	34.72	0.90
22.5	0.9503	4.6206	1.8020	9.53	1.30	0.0923	32.45	2.90	9.22	5.86	0.0757	34.85	0.80
22.5	0.9491	2.3775	2.7238	9.90	0.85	0.0912	32.50	2.88	9.71	3.43	0.0621	35.01	0.70
22.5	0.9493	0	3.7627	10.87	0.362	0.0720	32.52	2.77	10.72	2.81	0.0549	36.57	0.57
50	0.9513	8.8990[a]	0	8.59	1.88	0.115	29.34	2.98	8.37	6.59	0.0914	30.99	1.1
50	0.9511	8.8992	0	8.68	1.51	0.119	29.19	2.90	8.42	5.44	0.0944	30.83	1.2
50	0.9503	8.3166	0.2757	8.74	1.17	0.113	28.84	2.98	8.44	4.90	0.0902	30.71	1.2
50	0.9491	6.9732	0.8479	8.96	0.928	0.108	29.02	3.00	8.51	4.72	0.0845	30.90	1.3
50	0.9501	4.6206	1.8020	9.38	0.620	0.0989	29.20	3.00	8.90	2.20	0.0698	30.62	1.3
50	0.9509	2.3775	2.7238	9.81	0.444	0.0879	29.39	2.96	9.46	1.28	0.0586	30.93	1.0
50	0.9508	0	3.7627	10.62	0.335	0.0747	30.32	2.84	10.25	1.12	0.0506	31.95	0.90
75	0.9530	8.8990[a]	0	8.77	0.503	0.110	26.30	2.84	8.70	0.534	0.0804	26.15	1.2
75	0.9415	8.8992	0	8.80	0.494	0.116	26.34	2.83	8.74	0.458	0.0791	25.95	1.2
75	0.9473	8.3166	0.2757	8.84	0.437	0.113	26.18	2.84	8.74	0.475	0.0824	26.04	1.3
75	0.9503	6.9732	0.8479	8.97	0.458	0.107	26.59	2.83	8.76	0.449	0.0773	25.97	1.3
75	0.9492	4.6206	1.8020	9.30	0.304	0.0981	26.49	2.84	8.93	0.461	0.0672	26.52	1.4
75	0.9524	2.3775	2.7238	9.71	0.224	0.0860	26.60	2.90	9.36	0.289	0.0571	26.53	1.3
75	0.9478	0	3.7627	10.04	0.204	0.0772	27.05	2.84	9.75	0.242	0.0491	26.91	1.1

[a] In addition, 4.9 ml of 1 N HCl was added to these initial reactive fluids.

to obtain unambiguous dissolution rates from the temporal evolution of aqueous Mg concentrations (see Fig. 2). In contrast, the temporal evolution of aqueous Mg concentrations during precipitation was sufficiently slow to fit these data thereby retrieving hydromagnesite rates. Surface area-normalized hydromagnesite precipitation rates (r_{Hmg}) were fitted assuming they were consistent with surface growth in accord with:

$$r_{Hmg} = k_{Hmg}\left(\Omega_{Hmg}^{\frac{1}{\nu}} - 1\right)^{n} \quad (4)$$

where k_{Hmg} refers to a rate constant, Ω_{Hmg} represents the saturation state of the aqueous phase with respect to the precipitating hydromagnesite, ν refers to the stoichiometric number of activated species in one mole of hydromagnesite (= 5; Gautier *et al*., 2014) and *n* stands for the reaction order (= 1; Gautier *et al*., 2014). Measured aqueous Mg concentrations were fitted following the method described by Harouiya *et al*. (2007) using equation 4 and a trial-and-error method by varying k_{Hmg} and comparing fluid concentrations calculated using an EXCEL spread sheet with measured aqueous Mg concentrations. The results of this fit for all experiments are shown in Fig. 3, where it can be seen that the calculated curves provide a close description of the temporal variation of the measured aqueous Mg concentrations. Note that in some cases the first few measured Mg concentrations during a precipitation leg plot below the curve. This observation may be due to the effects of hydromagnesite nucleation on aqueous fluid concentrations. Nucleation, which is favoured in highly supersaturated fluids, is typically faster than growth and more strongly dependent on fluid saturation state. As such, aqueous Mg concentrations in fluids experiencing hydromagnesite nucleation will decrease faster with time than Mg concentrations in fluids experiencing only growth.

Hydromagnesite precipitation-rate constants, consistent with the regression curves shown in Fig. 3, are provided as a function of pH in Fig. 4. (1) Hydromagnesite precipitation-rate constants decrease by a factor of ~2 with increasing pH from 8.6 to 10.7 at 22.5ºC. A similar decrease in precipitation rates with pH was observed for the case of magnesite at 100 to 200ºC by Saldi *et al*. (2012). (2) Hydromagnesite precipitation-rate constants increase slightly with increasing temperature from 22.5 to 75ºC.

The final steady-state aqueous Mg concentrations during the dissolution and precipitation leg of each experiment were used together with corresponding pH and alkalinity values to determine the final *IAP* of hydromagnesite. The resulting *IAP* values are illustrated as a function of pH in Fig. 5. As these values were obtained from both dissolution and precipitation experiments, they bracket the equilibrium constant of the hydromagnesite hydrolysis reaction 1. The equilibrium *IAP* values shown in Fig. 5 were determined by the requirement that the equilibrium *IAP* be greater than those measured for dissolution and lower than those measured from precipitation. In each case, the equilibrium *IAP* was chosen as the largest highest *IAP* value determined from dissolution and the lowest determined from precipitation. There is some overlap among the measured *IAP* values for the 75ºC experiments, possibly due to uncertainties in the thermodynamic database adopted in this study. The logarithms of equilibrium constants for reaction 1 generated by equating K_{Hmg} to this equilibrium *IAP* (see equation 3) are 33.7 ± 0.9, 30.5 ± 0.5 and 26.5 ± 0.5, for 22.5, 50 and 75ºC, respectively.

Discussion

The role of hydromagnesite precipitation rates in mineral carbonation

The carbonation of Mg-rich olivine dissolution has been studied widely (e.g. Béarat *et al*., 2006; Andreani *et al*., 2009; Prigiobbe *et al*., 2009; King *et al*., 2010; Daval *et al*., 2011). Olivine is commonly thought to be the best source of the divalent metal cations required to create carbonate minerals due to its fast dissolution rates and worldwide abundance. The carbonation of Mg-enriched fluids due to forsterite dissolution at low temperatures, where magnesite precipitation is kinetically not favoured (e.g. Saldi *et al*., 2009), can proceed *via*:

$$\underset{\text{Forsterite}}{5Mg_2SiO_{4(s)}} + 8CO_{2(g)} + 20H_2O = \underset{\text{Hydromagnesite}}{2Mg_5(CO_3)_4(OH)_2{\cdot}4H_2O_{(s)}} + 5H_4SiO_{4(aq)} \quad (5)$$

Forsterite dissolution has been shown to follow a relatively simple dissolution mechanism (Pokrovsky and Schott, 2000; Oelkers, 2001); dissolution rates of forsterite have been reported by Wogelius and Walther (1991), Pokrovsky and Schott (2000), Oelkers (2001) and Hänchen *et al*. (2006) as a function of reactive fluid pH. At steady state, the stoichiometry of reaction 5 requires:

https://doi.org/10.1180/minmag.2014.078.6.07 Published online by Cambridge University Press

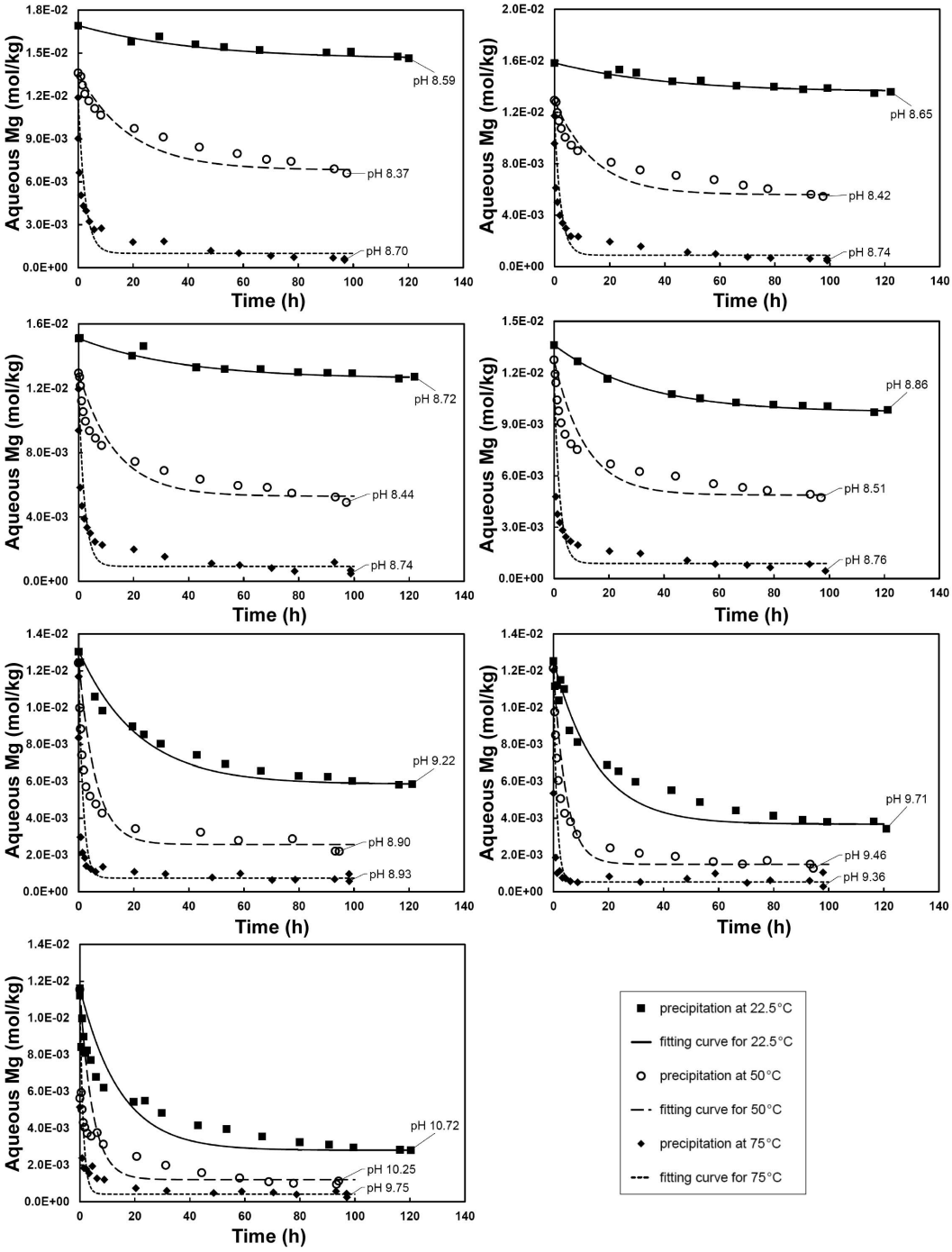

FIG. 3. Temporal evolution of aqueous Mg concentration during all experiments performed in this study. Results obtained at 22.5, 50 and 75ºC are represented by filled squares, hollow circles and filled diamonds, respectively. Fits of these data at 22.5, 50 and 75ºC are depicted by closed, dashed and dotted curves, respectively (see text).

https://doi.org/10.1180/minmag.2014.078.6.07 Published online by Cambridge University Press

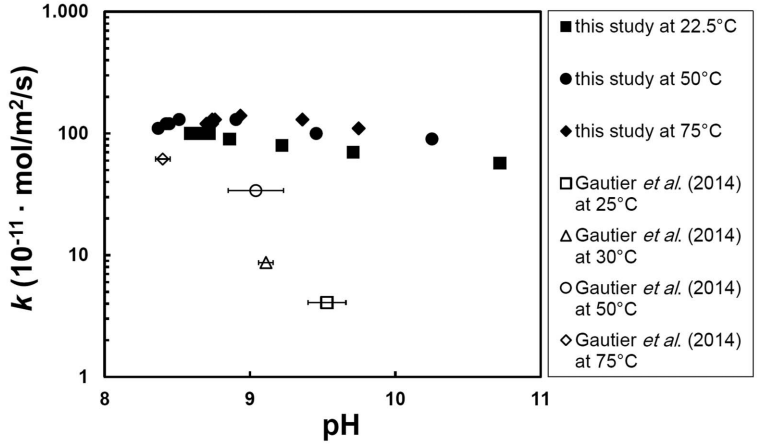

FIG. 4. Hydromagnesite precipitation rate constants as a function of pH. Constants for 22.5, 50 and 75ºC are represented by filled squares, circles and diamonds, respectively. Rate constants at different temperatures (published by Gautier *et al*., 2014) as a function of pH are plotted for comparison.

$$5r_{Fo}s_{Fo} = 2r_{Hmg}s_{Hmg} \quad (6)$$

where r_{Fo} and s_{Fo} refer to the surface area-normalized dissolution rate and surface area of forsterite, respectively, and sHmg stands for the surface area of hydromagnesite. A comparison of surface area-normalized forsterite dissolution rates and hydromagnesite precipitation rates is shown in Fig. 6. Forsterite dissolution rates after normalization to its Mg content are ~2 orders of magnitude slower than corresponding hydromagnesite precipitation rates. This observation indicates that, in contrast to the carbonation of forsterite to form magnesite (Saldi *et al*., 2009), the limiting step of the carbonation process to form hydromagnesite from forsterite is the relatively slow dissolution of forsterite. As forsterite dissolution rates are not increased by changing saturation state at far-from-equilibrium conditions (cf. Oelkers *et al*., 2001) or substantially by the addition of organic ligands (Declercq *et al*., 2013), it seems likely that the most efficient way of accelerating this overall process would be by increasing forsterite reactive surface areas (e.g. by increased grinding leading to reduced particle sizes).

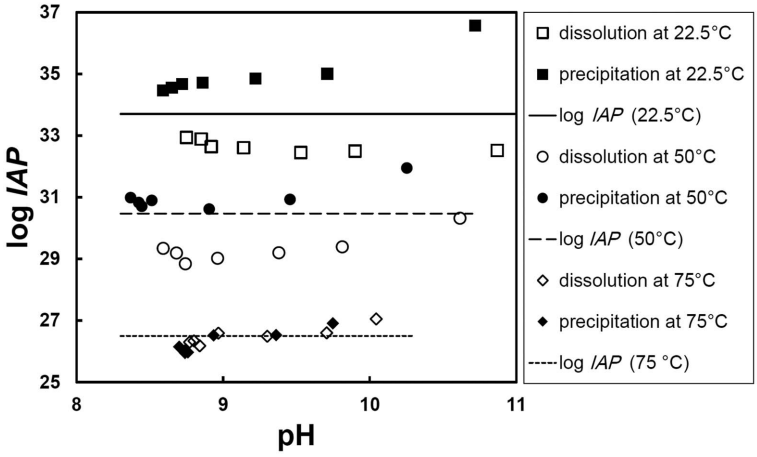

FIG. 5. Hydromagnesite ion activity products (IAP_{Hmg}) of the final fluid sampled of each experiment as a function of pH. Values of IAP_{Hmg} determined from 22.5, 50 and 75ºC experiments are portrayed by squares, circles and diamonds, respectively. Mean equilibrium *IAP* values are depicted by the solid lines indicated (see text).

https://doi.org/10.1180/minmag.2014.078.6.07 Published online by Cambridge University Press

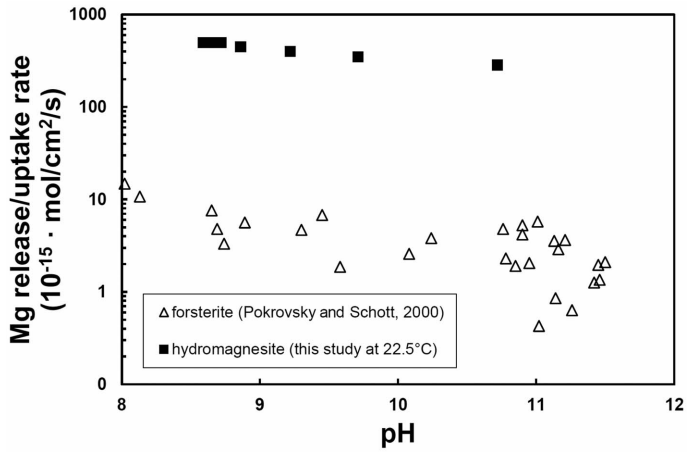

FIG. 6. Comparison of forsterite dissolution rates (Pokrovsky and Schott, 2000) *vs*. hydromagnesite precipitation rates (this study). All rates shown here are normalized to Mg release rather than to moles of mineral dissolved. These rates were obtained by multiplying reported mineral rates by the number of Mg atoms in the formula of each mineral.

Comparison with hydromagnesite hydrolysis constants available in the literature

As experiments reported in this study bracket equilibrated hydromagnesite from both undersaturated and supersaturated conditions, the results presented above constrain strongly the equilibrium constant of reaction 1. There have been few reports of hydromagnesite solubility measurements in the literature. Data present in the llnl database of *PHREEQC* originate from *SUPCRT92* (Johnson *et al*., 1992), which takes account of the thermodynamic properties of hydromagnesite reported by Helgeson *et al*. (1978), which themselves are based on the calorimetric measurements of Robie and Hemingway (1972, 1973). The equilibrium constants for reaction 1 as calculated using *PHREEQC* and its llnl database as a function of temperature are plotted in Fig. 7. Gautier *et al*.

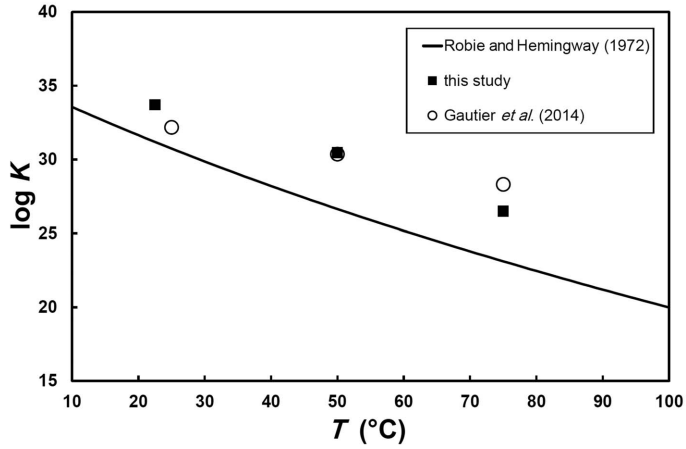

FIG. 7. Equilibrium constants for the hydromagnesite hydrolysis reaction (reaction 1) as a function of temperature. The results from the present study are represented by filled squares and can be compared to correponding values reported by Gautier *et al*. (2014) and those generated by themodynamic measurements by Robie and Hemingway (1972, 1973). Note that the solubility constant at 75ºC, reported by Gautier *et al*. (2014), was extrapolated rather than measured directly.

https://doi.org/10.1180/minmag.2014.078.6.07 Published online by Cambridge University Press

(2014) reported the hydromagnesite hydrolysis constants based on dissolution experiments performed on natural abiotic hydromagnesite. Measured equilibrium constants on natural biologically induced hydromagnesite, as determined in the present study, are 1–3 orders of magnitude greater than those generated from the Robie and Hemingway (1972, 1973) calorimetric data. Although these differences may be within the uncertainty of the calculations (c.f. Oelkers *et al*., 2009), such differences may also result from the presence of small hydromagnesite grains. Hydrolysis constants generated in this study are less than an order of magnitude different from those reported by Gautier *et al*. (2014), confirming these previous results, and suggesting a similar stability of biotic *vs*. abiotic hydromagnesite.

The variation of hydromagnesite precipitation rates as a function of temperature

The hydromagnesite precipitation rates illustrated in Fig. 4 suggest that there is little effect of increasing temperature on rates from 22.5 to 75ºC. This atypical observation can stem from a decrease in the number of active sites on the hydromagnesite surface in the higher-temperature experiments. A potential mechanism for the decrease in reactive surface area with increasing temperature is the agglomeration of hydromagnesite particles during precipitation. Particle agglomeration decreases rates by decreasing the hydromagnesite surface area in contact with the reactive fluid. Indeed, SEM images taken after the 22.5 and 75ºC experiments can be compared in Fig. 1, where it can be seen that the hydromagnesite recovered following the higher-temperature experiments are larger, potentially reflecting the increased agglomeration of these grains. Note also that Pokrovsky *et al*. (2009) and Schott *et al*. (2009) reported that carbonate mineral dissolution rates even decreased with increasing temperature from 100 to 150ºC. They attributed this atypical behaviour to changes in the surface speciation of carbonate minerals with increasing temperature.

A comparison between hydromagnesite precipitation-rate constants generated in the present study and those of Gautier *et al*. (2014) is also provided in Fig. 4. Rate constants generated in the present study on biogenic hydromagnesite are ~20 times faster than corresponding rate constants reported by Gautier *et al*. (2014) on abiotic hydromagnesite. This difference suggests that biogenic hydromagnesite has far more active sites per unit surface area than its abiotic counterpart. Comparison of photomicrographs presented by Gautier *et al*. (2014) and those from the present study shows the abiotic hydromagnesite to consist of euhedral and larger crystals. Note that rates at 75ºC reported for the biotic and abiotic hydromagnesite are similar in value, but as mentioned above, rates generated at this temperature in the present study may have been reduced due to agglomeration.

Conclusions

The results summarized above confirm the rapid dissolution and precipitation kinetics of hydromagnesite. Hydromagnesite dissolution rates were so rapid that they could not be quantified accurately from the closed-system reactor experiments performed in this study. Due to its rapid reaction rates, hydromagnesite should equilibrate quickly with low- and ambient-temperature natural fluids. The fast precipitation rates of hydromagnesite suggest that it could be an efficient product phase for the *ex situ* and *in situ* sequestration of CO_2.

Acknowledgements

The authors thank Vasilis Mavromatis for insightful discussions and encouragement, Carol Causserand for her help with wet-chemical analysis, Thierry Aigouy for technical support in obtaining SEM images and Michell Thibaut for X-ray analysis. This study was supported by the Centre National de la Recherche Scientifique (CNRS), the European Commission (through Marie Cuire ITN project MINSC, 290040; and PROCOPE – DAAD 55923335/Egide 28469SD).

References

Alfredsson, H.A., Hadrarson, B.S., Franzson, H. and Gislason, S.R. (2008) CO_2 sequestration in basaltic rock at the Hellisheidi site in SW Iceland: stratigraphy and chemical composition of the rocks at the injection site. *Mineralogical Magazine*, **72**, 1–5.

Andreani, M., Luquot, L., Gouze, P., Godard, M., Hoise, E. and Gibert, B. (2009) Experimental study of carbon sequestration reactions controlled by the percolation of CO_2-rich brine through peridotites.

https://doi.org/10.1180/minmag.2014.078.6.07 Published online by Cambridge University Press

Environmental Science & Technology, **43**, 1226–1231.

Aradóttir, E.S.P., Sonnenthal, E.L., Björnsson, G. and Jónsson, H. (2012) Multidimensional reactive transport modeling of CO_2 mineral sequestration in basalts at the Hellisheidi geothermal field, Iceland. *International Journal of Greenhouse Gas Control*, **9**, 24–40.

Béarat, H., McKelvy, M.J., Chizmeshya, A.V.G., Gormley, D., Nunez, R., Carpenter, R.W., Squires, K. and Wolf, G.H. (2006) Carbon sequestration via aqueous olivine mineral carbonation: Role of passivating layer formation. *Environmental Science & Technology*, **40**, 4802–4808.

Brown, P.L., Drummond, S.E. and Palmer, D.A. (1996) Hydrolysis of magnesium (II) at elevated temperatures. *Journal of the Chemical Society-Dalton Transactions*, **1996**, 3071–3075.

Brunauer, S., Emmett, P. and Teller, E. (1938) Adsorpotion of gases in multimolecular layers. *Journal of the American Chemical Society*, **60**, 309–319.

Burton, E.A. and Walter, L.M. (1987) Relative precipitation rates of aragonite and Mg calcite from seawater – temperature or carbonate control. *Geology*, **15**, 111–114.

Daval, D., Sissmann, O., Menguy, N., Saldi, G.D., Guyot, F., Martinez, I., Crovixier, J., Garcia, B., Machouk, I., Knauss, K. and Hellmann, R. (2011) Influence of amorphous silica layer formation on the dissolution rate of olivine at 90ºC and elevated pCO_2. *Chemical Geology*, **284**, 193–209.

Declercq, J., Bosc, O. and Oelkers, E.H. (2013) Do organic acids affect forsterite dissolution rates? *Applied Geochemistry*, **39**, 69–77.

Flaathen, T.K., Oelkers, E.H., Gislason, S.R. and Aagaard, P. (2011) The effect of dissolved sulphate on calcite precipitation kinetics and consequences for subsurface CO_2 storage. *Energy Procedia*, **4**, 5037–5043.

Gautier, Q., Bénézeth, P., Mavromatis, V. and Schott, J. (2014) Hydromagnesite solubility product and growth kinetics in aqueous solution from 25 to 75ºC. *Geochimica et Cosmochimica Acta*, **138**, 1–20.

Gislason, S.R. and Oelkers, E.H. (2014) Carbon storage in basalt. *Science* **344**, 373–374.

Gislason, S.R., Wolff-Boenisch, D., Stefansson, A., Oelkers, E.H., Gunnlaugsson, E., Sigurdardóttir, H., Sigfússon, G., Brocker, W.S., Matter, J., Stute, M., Axelsson, G. and Fridriksson, T. (2010) Mineral sequestration of carbon dioxide in basalt: A pre-injection overview of the CarbFix project. *International Journal of Greenhouse Gas Control*, **4**, 537–545.

Gysi, A.P. and Stefansson, A. (2012) CO_2–water–basalt interaction. Low-temperature experiments and implications for CO_2 sequestration into basalts. *Geochimica et Cosmochimica Acta*, **81**, 129–152.

Hänchen, M., Prigiobbe, V., Storti, G., Seward, T.M. and Mazzotti, M. (2006) Dissolution kinetics of fosteritic olivine at 90–150ºC including effects of the presence of CO_2. *Geochimica et Cosmochimica Acta*, **70**, 4403–4416.

Harouiya, N., Chairat, C., Kohler, S.K. and Oelkers, E.H. (2007) The dissolution kinetics and apparent solubility of natural apatite in close system reactors at temperatures from 5 to 50ºC and pH from 1 to 6. *Chemical Geology*, **244**, 554–568.

Helgeson, H.C., Delaney, J.M., Nesbitt, H.W. and Bird, D.K. (1978) Summary and critique of the thermodynamic properties of rock forming minerals. *American Journal of Science*, **278A**, 1–228.

Johnson, J.W., Oelkers, E.H. and Helgeson, H.C. (1992) *SUPCRT92*: A software package for calculating the standard molal properties of minerals gases, aqueous species and reactions among them from 1 to 5000 bars and 0 to 1000ºC. *Computers & Geosciences*, **18**, 899–947.

King, H.E., Plümper, O. and Putnis, A. (2010) Effect of secondary phase formation on the carbonation of olivine. *Environmental Science & Technology*, **44**, 6503–6509.

Lackner, K.S., Wendt, C.H., Butt, D.P., Joyce, E.L. and Sharp, D.H. (1995) Carbon dioxide disposal in carbonate minerals. *Energy*, **20**, 1153–1170.

Lakshtanov, L.Z. and Stipp, S.L.S. (2010) Interaction between silica and calcium carbonate: 1. Spontaneous precipitation of calcium carbonate in the presence of dissolved silica. *Geochimica et Cosmochimica Acta*, **74**, 2655–2664.

Marini, L. (2007) *Geological Sequestration of Carbon Dioxide: Thermodynamics, Kinetics, and Reaction Path Modeling*. Elsevier, Amsterdam, 470 pp.

Matter, J.M., Broecker, W.S., Stute, M., Gislason, S.R., Oelkers, E.H., Stefansson, A., Wolff-Boenisch, D., Gunnlaugsson, E., Axelsson, G. and Bjornsson, G. (2009) Permanent carbon dioxide storage into basalt: The CarbFix pilot project Iceland. *Energy Procedia*, **1**, 3641–3646.

Matter, J.M., Broecker, W.S., Gislason, S.R., Gunnlaugsson, E., Oelkers, E.H., Stute, M., Sigurdardottir, H., Stefansson, A., Alfredsson, H.A., Aradottir, E.S., Axelsson, G., Sigfusson, B. and Wolff-Boenisch, D. (2011) The CarbFix Pilot Project – Storing Carbon Dioxide in basalt. *Energy Procedia*, **4**, 5579–5585.

Mavromatis, V., Pearce, C.R., Shirokova, L.S., Bundeleva, I.A., Pokrovsky, O.S., Bénézeth, P. and Oelkers, E.H. (2012) Magnesium isotope fractionation during hydrous magnesium carbonate precipitation with and without cyanobacteria. *Geochimica et Cosmochimica Acta*, **76**, 161–174.

https://doi.org/10.1180/minmag.2014.078.6.07 Published online by Cambridge University Press

McGrail, B.P., Schaef, H.T., Ho, A.M., Chien, Y.J., Dooley, J.J. and Davidson, C.L. (2006) Potential for carbon dioxide sequestration in flood basalts. *Journal of Geophysical Research: Solid Earth*, **111**, B12, DOI: 10.1029/2005JB004169.

Millero, F., Huang, F., Graham, T. and Pierrot, D. (2007) The dissociation of carbonic acid in NaCl solutions as a function of concentration and temperature. *Geochimica et Cosmochimica Acta*, **71**, 46–55.

Oelkers, E.H. (2001) An experimental study of forsterite dissolution rates as a function of temperature and aqueous Mg and Si concentrations. *Chemical Geology*, **175**, 485–494.

Oelkers, E.H., Gislason, S.R. and Matter, J. (2008) Mineral carbonation of CO_2. *Elements*, **4**, 333–337.

Oelkers, E.H., Bénézeth, P. and Pokrovsky, G.S. (2009) Thermodynamic databases for water–rock interaction. Pp. 1–46 in: *Thermodynamics and Kinetics of Water–Rock Interaction* (E.H. Oelkers and J. Schott, editors). Reviews in Mineralogy and Geochemistry, **70**, Mineralogical Society of America and the Geochemical Society, Chantilly, Virginia, USA.

Oskierski, H.C., Dlugogorski, B.Z. and Jacobsen, G. (2013) Sequestration of atmospheric CO_2 in chrysotile mine tailings of the Woodsreef Asbestos Mine, Australia: Quantitative mineralogy, isotopic fingerprinting and carbonation rates. *Chemical Geology*, **358**, 156–169.

Parkhurst, D.L. and Appelo, C.A.J. (1999) User's guide to *PHREEQC* (version 2) – A computer program for speciation, batch-reaction, one-dimensional transport, and inverse geochemical calculations. U.S. Geological Survey Water-resources Investigation Report 99-4259, pp. 312.

Pokrovsky, O.S. and Schott, J. (2000) Kinetics and mechanism of forsterite dissolution at 25ºC and pH from 1 to 12. *Geochimica et Cosmochimica Acta*, **64**, 3313–3325.

Pokrovsky, O.S., Golubev, S.V., Schott, J. and Castillo, A. (2009) Calcite, dolomite and magnesite dissolution kinetics in aqueous solutions at acid to circumneutral pH, 25 to 150ºC and 1 to 55 atm pCO_2: New constraints on CO_2 sequestration in sedimentary basins. *Chemical Geology*, **265**, 20–32.

Prigiobbe, V., Hänchen, M., Werner, M., Baciocchi, R. and Mazzotti, M. (2009) Mineral carbonation processes for CO_2 sequestration. *Energy Procedia*, **1**, 4885–4890.

Robie, R.A. and Hemingway, B.S. (1972) The heat capacities at low temperatures and entropies at 298.15 K of nesquehonite, $MgCO_3{\cdot}3H_2O$, and hydromagnesite. *American Mineralogist*, **57**, 1768–1781.

Robie, R.A. and Hemingway, B.S. (1973) The enthalpies of formation of nesquehonite, $MgCO_3{\cdot}3H_2O$, and hydromagnesite, $5MgO{\cdot}4CO_2{\cdot}5H_2O$. *Journal of Research of the U.S. Geological Survey*, **1**, 543–547.

Rodriguez-Blanco, J.D., Shaw, S. and Benning, L.G. (2011) The kinetics and mechanism of amorphous calcium carbonate (ACC) crystallization to calcite. *Nanoscale*, **3**, 265–271.

Ruiz-Agudo, E., Kudlacz, K., Putnis, C.V., Putnis, A. and Rodriguez-Navarro, C. (2013) Dissolution and carbonation of portlandite ($Ca(OH)_2$) single crystals. *Environmental Science & Technology*, **47**, 11342–11349.

Saldi, G.D., Jordan, G., Schott, J. and Oelkers, E.H. (2009) Magnesite growth rates as a function of temperature and saturation state. *Geochimica et Cosmochimica Acta*, **73**, 5646–5657.

Saldi, G.D., Schott, J., Pokrovsky, O.S., Gautier, Q. and Oelkers, E.H. (2012) An experimental study of magnesite precipitation rates at neutral to alkaline conditions and 100–200ºC as a function of pH, aqueous solution composition and chemical affinity. *Geochimica et Cosmochimica Acta*, **83**, 93–109.

Schaef, H.T., McGrail, B.P. and Owen, A.T. (2010) Carbonate mineralization of volcanic province basalts. *International Journal of Greenhouse Gas Control*, **4**, 249–261.

Schaef, H.T., McGrail, B.P. and Owen, A.T. (2011) Basalt reactivity variability with reservoir depth in supercritical CO_2 and aqueous phases. *Energy Procedia*, **4**, 4977–4984.

Schott, J., Pokrovsky, O.S. and Oelkers, E.H. (2009) The link between mineral dissolution/precipitation kinetics and solution chemistry. Pp. 207–258 in: *Thermodynamics and Kinetics of Water–Rock Interaction* (E.H. Oelkers and J. Schott, editors). Reviews in Mineralogy and Geochemistry, **70**, Mineralogical Society of America and the Geochemical Society, Chantilly, Virginia, USA.

Seifritz, W. (1990) CO_2 disposal by means of silicates. *Nature*, **345**, 486.

Shirokova, L.S., Mavromatis, V., Bundeleva, I., Pokrovsky, O.S., Bénézeth, P., Pearce, C., Gerard, E., Balor, S. and Oelkers, E.H. (2011) Can Mg isotopes be used to trace cyanobacteria-mediated magnesium carbonate precipitation in alkaline lakes? *Biogeosciences Discussions*, **8**, 6473–6517.

Shirokova, L.S., Mavromatis, V., Bundeleva, I.A., Pokrovsky, O.S., Bénézeth, P., Gerard, E., Pearce, C.R. and Oelkers, E.H. (2013) Using Mg isotopes to trace cyanobacterially mediated magnesium carbonate precipitation in alkaline lakes. *Aquatic Geochemistry*, **19**, 1–24.

Teng, H.H., Dove, P.M. and de Yoreo, J.J. (2000) Kinetics of calcite growth: Surface processes and relationships to macroscopic rate laws. *Geochimica et Cosmochimica Acta*, **64**, 2255–2266.

https://doi.org/10.1180/minmag.2014.078.6.07 Published online by Cambridge University Press

Wogelius, R.A. and Walther, J.V. (1991) Olivine dissolution at 25ºC: effects of pH, CO_2 and organic acids. *Geochimica et Cosmochimica Acta*, **55**, 943–954.

Xu, T.F., Apps, J.A. and Pruess, K. (2005) Mineral sequestration of carbon dioxide in a sandstone–shale system. *Chemical Geology*, **217**, 295–318.

Zuddas, P. and Mucci, A. (1998) Kinetics of calcite precipitation from seawater: II Influence of the ionic strength. *Geochimica et Cosmochimica Acta*, **62**, 757–766.

https://doi.org/10.1180/minmag.2014.078.6.07 Published online by Cambridge University Press